Available online at www.sciencedirect.com

ScienceDirect

Geochimica et Cosmochimica Acta 316 (2022) 347–362

Geochimica et Cosmochimica Acta

www.elsevier.com/locate/gca

Effective global mixing of the highly siderophile elements into Earth's mantle inferred from oceanic abyssal peridotites

Marine Paquet [a,b,*], James M.D. Day [a], Diana B. Brown [a], Christopher L. Waters [a]

[a] Scripps Institution of Oceanography, University of California San Diego, La Jolla, CA 92093, USA
[b] Institut de Physique du Globe de Paris, UMR 7154 CNRS, Université de Paris, 1 rue Jussieu, 75238 Paris, France

Received 20 April 2021; accepted in revised form 27 September 2021; Available online 5 October 2021

Abstract

Late accretion occurred through addition of massive impactors to Earth, leading to potential heterogeneity in the distribution of highly siderophile elements (HSE: Os, Ir, Ru, Pt, Pd, Re) within the mantle. Abyssal peridotites sample the present-day convecting mantle, which make them useful for examining the distribution of the HSE within the mantle. Here we report new HSE abundance data and $^{187}Os/^{188}Os$ ratios, in conjunction with mineral chemistry and bulk rock major- and trace-element compositions for abyssal peridotites from the fast-spreading Pacific Antarctic Ridge (PAR) and East Pacific Rise (Hess Deep), and for slow to intermediate spreading ridges from the Southwest Indian Ridge, Central Indian Ridge and Mid-Atlantic Ridge. These analyses expand the global abyssal peridotite Os isotope and HSE database, enabling evaluation of potential variations with spreading rate, from ultraslow (<20 mm/yr, full spreading rate) to fast (135–150 mm/yr). Accounting for likely effects from seawater modification and serpentinization, the Pacific data reveals heterogeneous and sometimes significant melt depletion for PAR (3–23% melt depletion; $^{187}Os/^{188}Os$ from 0.1189 to 0.1336, average = 0.1267 ± 0.0065; 2SD) and Hess Deep abyssal peridotites (15–20% melt depletion; 0.1247 ± 0.0027). Abyssal peridotites from fast to intermediate spreading ridges reveal no systematic differences in the distribution and behavior of the HSE or Os isotopes, or in degrees of melt depletion, compared with slow to ultraslow spreading ridges. These observations arise despite significant differences in melt generation processes at mid-ocean ridges, suggesting that the effects of ancient melt depletion are more profound on HSE compositions in abyssal peridotites than modern melting beneath ridges. Using global abyssal peridotites with Al_2O_3 content > 2 wt.%, the average composition of the primitive mantle is 0.3 ppb Re, 4.9 ppb Pd, 7.1 ppb Pt, 7.2 ppb Ru, 3.8 ppb Ir and Os, showing no Pd/Ir, but a positive Ru/Ir anomaly, relative to chondrites. There is ~50% variation of the HSE abundances in the oceanic mantle, with much of this variation being observed at small length scales (<1 km) and due entirely to both modern and more ancient partial melting effects. Consequently, any significant HSE heterogeneities formed during late accretion or early Earth differentiation processes are no longer recognizable in the mantle sampled within ocean basins, implying generally efficient mixing of Earth's mantle for these elements. By contrast, relatively ancient heterogeneity in Os and other radiogenic isotopes has been effectively preserved in the convecting mantle over the last ~2 Ga, through recycling processes and through preservation and isolation of melt-depleted refractory residues.

Keywords: Oceanic mantle; Peridotite; Highly siderophile elements; Os isotopes; Late accretion; Mantle convection; Heterogeneity

1. INTRODUCTION

The highly siderophile elements (HSE: Os, Ir, Ru, Pt, Rh, Pd, Re, Au) are key geochemical tools with which to investigate terrestrial accretion and differentiation

* Corresponding author at: Scripps Institution of Oceanography, University of California San Diego, La Jolla, CA 92093, USA.
E-mail addresses: mpaquet@ucsd.edu (M. Paquet), jmdday@ucsd.edu (J.M.D. Day).

https://doi.org/10.1016/j.gca.2021.09.033
0016-7037/

processes. The HSE are generally compatible during partial melting and are characterized by elevated metal-silicate partition coefficients at mantle pressures ($>10^4$; e.g., O'Neill et al., 1995; Holzheid et al., 2000; Ertel et al., 2001; Brenan and McDonough, 2009; Brenan et al., 2016; Suer et al., 2021 and references therein). Assuming such high partition coefficients, Earth's core and mantle are not in equilibrium for the HSE, and the mantle has abundances of these elements only ~150 times less abundant than in chondrites; some three orders of magnitude higher than expected (Morgan, 1986; Snow and Schmidt, 1998; Morgan et al., 2001; Becker et al., 2006; Fischer-Gödde et al., 2011; Day et al., 2016a; 2017a).

Three main hypotheses have been suggested to explain this discrepancy: (1) the "late accretion" or "late veneer" hypothesis where addition of "chondritic" impactors occurred after the major phase(s) of core formation (e.g., Turekian and Clark, 1969; Kimura et al., 1974; Chou, 1978; Jagoutz et al., 1979; Wänke, 1981; Meisel et al., 1996); (2) mixing or inefficient separation of differentiated outer-core material back into the mantle shortly after core separation (Jones & Drake, 1986; Snow & Schmidt, 1998), or; (3) lower metal-silicate partition coefficients at higher pressures and temperatures (HP-HT; e.g., Ringwood, 1977; Murthy, 1991). The late accretion model is generally the most popular given its ability to explain both the broadly chondritic $^{187}Os/^{188}Os$ as well as the elevated absolute abundances of the HSE that are in chondritic proportions within the bulk silicate Earth (BSE), requiring between ~0.5 and 0.8 wt.% addition of mass to Earth (Becker et al., 2006; Day et al., 2016a).

An outstanding question that remains, however, is how evenly distributed the HSE are within the present-day convecting mantle. Late accretion likely occurred through addition of massive impactors (Bottke et al., 2010), leading to the possibility of heterogeneous distribution of the HSE within Earth's mantle following late accretionary impacts, and enhanced deposition of impactor material within the mantle, perhaps at hemispheric scales, or at the scale of thousands of kilometers. For example, it has been demonstrated that metal-silicate equilibration differs depending on the target latitude of the impactor due to the influence of the planetary rotation on the mixing and settling history, which may generate chemical heterogeneities (e.g., HSE) and isotopic anomalies (e.g., ^{182}W anomalies) (Maas et al., 2021). For smaller planetary bodies, such as the probable asteroidal source of eucrite and diogenite meteorites, 4-Vesta, it has been proposed that the inferred patchy distribution of the HSE reflects regional rather than global late accretion effects shortly after planet formation (Day et al., 2012). In contrast, while Earth may have originally had a more heterogeneous distribution of the HSE within the mantle, compositional variations in mantle materials at the present-day are seemingly more consistent with homogeneous distributions through prolonged melting and/or solid-state convection. The evidence from mantle peridotites preserved in ophiolites is that there is more limited heterogeneity at > km length scales than at the scale of meters or less (e.g., O'Driscoll et al., 2012; Snortum & Day, 2020; Haller et al., 2021). Arguably, however, the ideal test of HSE homogeneity in Earth's mantle comes from the study of oceanic abyssal peridotites. Abyssal peridotites are samples of Earth's present-day convecting mantle sampled within ocean basins, so that provide a snap-shot of the degree of present-day HSE homogeneity within the mantle.

Prior attempts to estimate the HSE composition of Earth's mantle have assumed relative initial homogeneity to attain a BSE composition (equivalent to primitive mantle [PM] and referred to as primitive upper mantle [PUM] by Becker et al., 2006), with workers utilizing a range of mantle rock types, including ultramafic massifs and ophiolites (e.g., Becker et al., 2006; Zhang et al., 2020), as well as using abyssal peridotites (e.g., Becker et al., 2006; Day et al., 2017a). These approaches for determining the absolute and relative abundances of the HSE in the bulk silicate Earth, and the extent of heterogeneity have drawbacks. For example, utilizing massif compositions requires effective subtraction of the effects of sometimes complex melt refertilization processes (e.g., Marchesi et al., 2014; Becker and Dale, 2016; Lorand and Luguet, 2016). Abyssal peridotites represent residues of ancient and modern depletion events (2% to > 16%), which occurred > 0.5 Ga ago for some samples (e.g., Brandon et al., 2000; Harvey et al., 2006; Liu et al., 2008; Lassiter et al., 2014; Day et al., 2017a). Complications with these samples are that melt refertilization (e.g., Niu, 2004; Warren, 2016; Reisberg, 2021) and serpentinization or secondary alteration (e.g., Snow and Dick, 1995; Snow and Reisberg, 1995; Malvoisin, 2015) processes can affect their compositions. Furthermore, abyssal peridotites are difficult to sample, being either dredged or drilled typically from deep water locations (>3 km) and relatively rare exposures on the ocean floor, such that global coverage has hitherto not been obtained.

Currently, HSE and Os isotope data for abyssal peridotites are mainly from ultraslow to slow spreading ridges (e.g., Gakkel Ridge, Southwest Indian Ridge, Central Indian Ridge, Mid-Atlantic Ridge; Martin, 1991; Roy-Barman & Allègre, 1994; Snow & Reisberg, 1995; Snow & Schmidt 1998; Brandon et al., 2000; Luguet et al., 2001; 2003; Standish et al, 2002; Alard et al., 2005; Harvey et al., 2006; Sichel et al., 2008; Liu et al., 2008; 2009; Lassiter et al., 2014; Day et al., 2017a). More limited data are available on the HSE abundances and Os isotopic composition of mantle beneath intermediate and fast spreading centers (Roy-Barman and Allègre, 1994; Snow and Schmidt, 1998; Rehkämper et al., 1999). Here we report new bulk rock $^{187}Os/^{188}Os$ and HSE abundance data for abyssal peridotites from the Pacific Ocean (Hess Deep along the East Pacific Rise (EPR) and from the Udintsev Fracture Zone (UFZ) along the Pacific Antarctic Ridge (PAR)). We compare these data with those obtained for abyssal peridotites from ultraslow to slow spreading ridges (e.g., Gakkel Ridge, Southwest Indian Ridge (SWIR), Central Indian Ridge (CIR), Mid-Atlantic Ridge (MAR)). Additionally, new bulk rock major and trace element abundances and mineral chemistry are reported for some samples to examine the relationship to spreading rate and melt depletion in abyssal peridotites, and to assess heterogeneity of mantle composition in terms of HSE abundances

and Os isotope ratios, as well as the implications this might have for mantle geodynamics.

2. SAMPLES AND METHODS

2.1. Samples

Dredged abyssal peridotites were analyzed from the fast-spreading East Pacific Rise (EPR), at Hess Deep (denoted AII) from cruise 125, leg 6, aboard the RV Atlantis II in May 1990. Dredged abyssal peridotites were also analyzed from the Pacific Antarctic Ridge (PAR), along two different locations of the Udintsev ridge, denoted as WEST03-MV12 and WEST03-MV13, from the WESTWARD (WEST03MV) cruise aboard the RV Melville in February 1994. Details for this cruise are reported in Castillo et al. (1998) and Niu (2004). New data are also reported for abyssal peridotites from slower spreading rates (Mid-Atlantic Ridge, Central Indian Ridge and Southwest Indian Ridge) from the 1968 CIRCE cruise (Circe97) aboard the RV Argo, the 1970 ANTIPODE cruise (ANTP) aboard the RV Melville, the 1984 Protea Cruise (Prot05) aboard the RV Melville, the 1990 PLUME cruise (PLUM05) aboard the RV Thomas Washington, and the 2007 KNOX11RR cruise aboard the RV Roger Revelle. Sample locations are reported in Fig. 1 and Table 1.

2.2. Mineral compositions

Major- and minor-element mineral compositions were obtained from polished mounts containing olivine, pyroxene and spinel, and as polished thick sections for Hess Deep and PAR samples, using a JEOL JXA-8230 electron probe micro analyzer (EPMA) at the University of Colorado, USA (Department of Geological Sciences). Analyses were made with an accelerating potential of 15 keV and a beam size of 5 μm. Beam currents were 30 nA for olivine and pyroxene and 20 nA for spinel. Both natural and synthetic standards were used to calibrate the EMP and were measured throughout analytical sessions to ensure data quality. Background and peak counting times used were 20–30 s and standard PAP correction procedures were used. Detection limits were $\leq$ 0.02 wt.% for Si, Al, Mg, Ca, Na, K and P and $<$ 0.04 wt.% for Fe, Ti, Mn, V, Ni and Cr.

2.3. Bulk rock major and trace element abundance analyses

Major element compositions were measured by X-ray fluorescence (XRF) at Franklin and Marshall College using a PW 2404 PANalytical XRF vacuum spectrometer following the protocol described in Day et al. (2017a) and references therein. Repeated measurements of basaltic reference material BHVO-2 allow estimations of precision and accuracy, with long-term reproducibility of 0.1% for SiO_2, Al_2O_3, Fe_2O_{3T}, MgO and CaO, 0.2% for TiO_2, MnO and Na_2O, and 0.3% for P_2O_5 (Table S1).

Trace element analyses were performed on 100 mg of homogenized bulk rock powder using a Thermo Scientific iCAP Qc ICP-MS at the Scripps Isotope Geochemistry Laboratory (SIGL, University of California San Diego), following the method outlined in Day et al. (2014). Samples were analyzed with several replicates of powdered peridotites HARZ-01 and PLUM05-49, as well as BHVO-2, BCR-2 and BIR-1a, basaltic reference materials, used as standards to confirm accuracy, with reproducibility on most of trace element abundances better than 10% (Table S2).

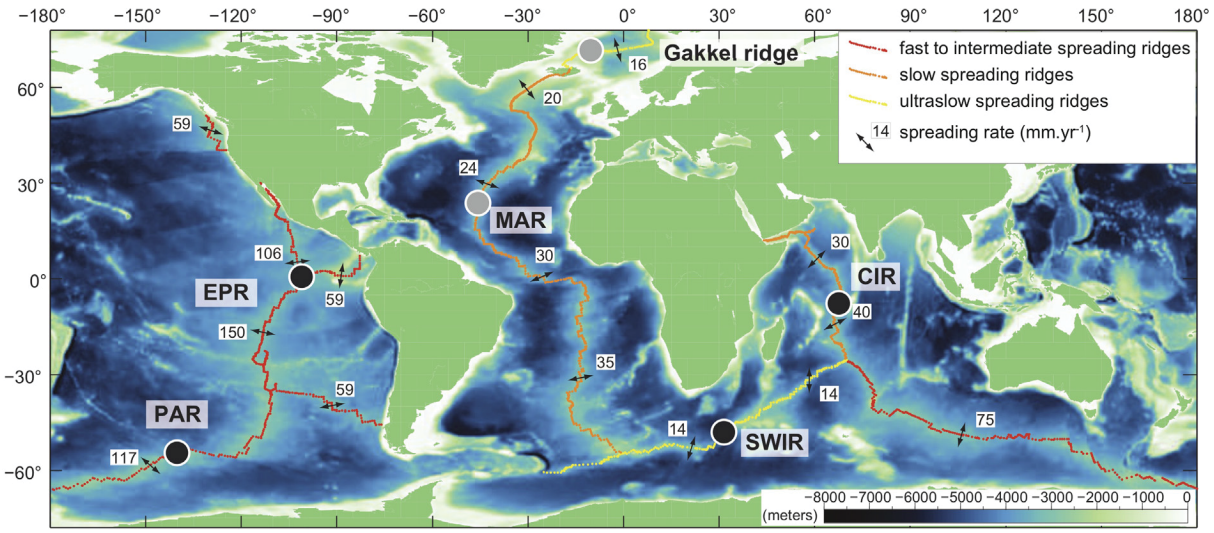

Fig. 1. Mid-ocean ridge full spreading rates and location of abyssal peridotites analyzed for Re-Os isotopes and HSE abundance systematics in this study (EPR, PAR, SWIR, CIR) and prior studies (modified from Rouméjon, 2014). Spreading rates are from DeMets et al. (1990). The black circles represent locations of new HSE and Os isotope data for abyssal peridotites from Hess Deep along the East Pacific Rise (EPR) and from the Udintsev fracture zone along the Pacific Antarctic Ridge (PAR), as well as from the Central and Southwest Indian Ridges. The light gray circles correspond to abyssal peridotite samples from other slower spreading centers (Snow and Schmidt, 1998; Brandon et al., 2000, 2006; Luguet et al., 2001, 2003; Becker et al., 2006; Liu et al., 2009; Lassiter et al., 2014; Day et al., 2017a; Li et al., 2019).

Table 1
Osmium isotope and highly siderophile element abundance data for Pacific abyssal peridotites.

Location and specimen	Description	Latitude (°)	Longitude (°)	Al_2O_3 (wt.%)	LOI (wt.%)	Re (ppb)	Pd (ppb)	Pt (ppb)	Ru (ppb)	Ir (ppb)	Os (ppb)	$^{187}Os/^{188}Os$	2σ	T_{RD}
Pacific Antartic Ridge (Udintsev Fracture Zone)														
WEST03MV-12-1-1	Udintsev FZ	-56.388	-142.432	1.76	10.3	0.154	6.179	5.925	7.675	4.834	4.100	0.12568	0.00014	552
WEST03MV-12-1-4	Udintsev FZ	-56.388	-142.432	2.07	11.2	0.425	6.839	8.149	9.766	5.486	4.775	0.12606	0.00009	499
WEST03MV-12-1-7	Udintsev FZ	-56.388	-142.432	1.82	9.8	0.279	6.136	5.289	7.031	4.404	3.558	0.12776	0.00010	260
WEST03MV-12-1-9	Udintsev FZ	-56.388	-142.432	1.84	11.9	0.373	8.383	7.893	9.930	5.060	4.571	0.12678	0.00011	397
WEST03MV-12-1-10	Udintsev FZ	-56.388	-142.432	3.94	9.5	0.807	9.540	9.347	8.497	5.415	4.629	0.13129	0.00009	-
WEST03MV-12-1-18	Udintsev FZ	-56.388	-142.432	2.33	12.7	0.871	6.397	6.818	8.101	4.463	4.084	0.12753	0.00015	292
WEST03MV-12-1-29	Udintsev FZ	-56.388	-142.432	1.17	13.7	0.123	2.428	4.341	5.943	3.426	2.048	0.11996	0.00011	1348
WEST03MV-12-1-32	Udintsev FZ	-56.388	-142.432	1.86	13.4	0.140	4.100	6.950	8.090	4.530	-	-	-	-
WEST03MV-12-1-59	Udintsev FZ	-56.388	-142.432	1.75	12.4	0.147	4.917	4.819	5.967	3.323	2.743	0.12574	0.00013	544
WEST03MV-12-1-61	Udintsev FZ	-56.388	-142.432	1.79	12.8	0.179	7.632	6.913	8.582	5.163	4.078	0.12273	0.00015	965
WEST03MV-12-1-66	Udintsev FZ	-56.388	-142.432	2.35	11.6	0.301	5.657	6.462	7.532	4.725	3.897	0.12621	0.00014	478
WEST03MV-12-1-67	Udintsev FZ	-56.388	-142.432	1.99	8.2	0.262	6.565	6.822	7.854	4.768	3.859	0.12774	0.00009	262
WEST03MV-12-1-70	Udintsev FZ	-56.388	-142.432	2.68	5.7	0.736	7.416	10.67	9.450	5.421	5.056	0.12741	0.00009	309
WEST03MV-12-1-71	Udintsev FZ	-56.388	-142.432	2.29	5.5	0.902	6.593	6.565	7.478	3.914	3.559	0.12774	0.00011	262
WEST03MV-13-4-1	Udintsev FZ	-56.542	-141.967	2.09	6.4	0.166	7.461	7.513	7.690	3.743	4.181	0.12723	0.00010	334
WEST03MV-13-4-2	Udintsev FZ	-56.542	-141.967	2.08	7.7	0.097	5.200	7.003	7.647	4.633	3.824	0.12810	0.00010	212
WEST03MV-13-4-3	Udintsev FZ	-56.542	-141.967	2.97	8.3	0.586	13.28	12.81	12.16	6.573	6.018	0.13004	0.00010	-
WEST03MV-13-4-5	Udintsev FZ	-56.542	-141.967	1.81	8.2	0.156	3.675	7.446	8.914	5.362	4.988	0.12382	0.00009	812
WEST03MV-13-4-8	Udintsev FZ	-56.542	-141.967	2.19	4.9	0.066	7.798	5.815	6.647	3.348	2.900	0.13359	0.00020	-
WEST03MV-13-4-11	Udintsev FZ	-56.542	-141.967	2.23	7.2	0.112	5.199	6.580	8.198	4.942	3.705	0.13023	0.00010	-
WEST03MV-13-5-3	Udintsev FZ	-56.542	-141.967	1.79	9.8	0.054	6.529	6.038	7.049	3.589	2.225	0.12756	0.00008	288
WEST03MV-13-5-8	Udintsev FZ	-56.542	-141.967	2.08	11.9	0.122	4.726	5.609	7.416	3.934	2.993	0.12873	0.00012	123
WEST03MV-13-5-12	Udintsev FZ	-56.542	-141.967	1.49	9.0	0.054	4.093	6.085	7.896	5.320	5.248	0.11889	0.00009	1496
WEST03MV-13-5-13	Udintsev FZ	-56.542	-141.967	1.24	10.1	0.014	3.543	4.760	6.844	3.200	2.838	0.12391	0.00010	800
East Pacific Rise (Hess Deep)														
All-125-6-4D-18NV	Hess Deep	-2.28	-101.45	0.65	13.4	0.126	5.641	12.24	7.044	3.636	2.882	0.12515	0.00010	627
All-125-6-4D-18WV	Hess Deep	-2.28	-101.45	0.66	13.5	0.050	6.090	8.110	6.480	3.620	2.989	0.12389	0.00011	803
All-125-6-4D-41	Hess Deep	-2.28	-101.45	0.81	13.7	0.350	7.590	8.070	6.500	3.510	3.514	0.12718	0.00010	341
All-125-6-4D-42	Hess Deep	-2.28	-101.45	0.69	13.3	0.200	17.67	9.010	11.71	6.640	5.868	0.12435	0.00010	738
All-125-6-4D-43	Hess Deep	-2.28	-101.45	0.74	13.1	0.312	6.869	6.899	13.27	5.366	6.326	0.12318	0.00011	901
Southwest Indian Ridge														
PROT05-14D-65	Dutoit FZ	-53.102	25.318	2.19	13.2	0.130	1.434	7.927	6.805	4.930	3.921	0.12788	0.00009	243
Central Indian Ridge														
ANTP87D-CLW1	Marie Celeste FZ	-17.6	65.75	0.82	14.6	0.007	0.591	6.851	7.498	9.298	9.299	0.12259	0.00009	983
CIRCE97A	Marie Celeste FZ	-17.6	65.75	0.30	14.7	0.016	0.621	1.355	7.139	2.118	1.909	0.12314	0.00012	906
CIRCE97-HD-2	Marie Celeste FZ	-17.6	65.75	1.24	13.2	0.019	0.063	0.160	2.205	0.306	0.188	0.12803	0.00025	222
CIRCE97-HD-4	Marie Celeste FZ	-17.6	65.75	1.23	13.5	0.325	8.046	9.167	10.31	5.435	4.184	0.12892	0.00011	96
CIRCE93-HD-2	Marie Celeste FZ	-17.6	65.75	-	-	0.093	3.317	1.637	2.188	2.263	0.646	0.13267	0.00015	-

T_{RD} = Time of rhenium depletion age, calculated as: $1/\lambda \times \ln\{([^{187}Os/^{188}Os_{chondrite} - {}^{187}Os/^{188}Os_{sample}]/[^{187}Re/^{188}Os_{chondrite}])+1\}$.
Latitude and longitude are given in decimal degrees.

2.4. Highly siderophile elements and Os isotopic compositions

Osmium isotope and HSE abundance analyses were performed at the SIGL on ~900 mg of homogenized powder from a larger powder aliquot. The samples were precisely weighed and digested in sealed 20 cm borosilicate Carius tubes using a mixture of multiply Teflon distilled 12 M HCl (4 mL) and "purged" 15.7 M HNO_3 (7 mL; expunged of Os using H_2O_2), with isotopically enriched multi-element spikes (^{99}Ru, ^{106}Pd, ^{185}Re, ^{190}Os, ^{191}Ir, ^{194}Pt). Digestions lasted 72 h hours in an oven at a maximum temperature of 250 °C. Osmium was purified by extracting CCl_4 three times from the HCl/HNO_3, spike and sample mixture and then back extracting the Os from the CCl_4 using HBr (Cohen and Waters, 1996), with further purification by micro-distillation (Birck et al., 1997). The other HSE (Re, Pd, Pt, Ru, Ir) were recovered and purified from the residual solutions using anion exchange column chemistry (e.g., Day et al., 2016b).

Acquisition of Os isotopic compositions were performed on a Thermo Scientific Triton thermal ionization mass spectrometer in negative ion mode, with HSE abundances calculated from isotopic ratios of Ir, Ru, Pt, Pd and Re measured using a Thermo Scientific iCAP Qc ICP-MS coupled to a Cetac Aridus II desolvating nebulizer. Osmium data were appropriately oxide-, fractionation-, spike- and blank corrected. Precision for $^{187}Os/^{188}Os$, determined by repeated measurements of 35 to 70 pg loads of the UMCP Johnson-Matthey standard, was better than ± 0.2% (2SD; 0.11382 ± 0.00012; n = 10). These standard load sizes were smaller than unknown samples, which had > 1 ng Os, and that typically ran with signal sizes of 200 K Cps on the largest mass isotope, with stable signals similar to the standards. Rhenium, Pd, Pt, Ir and Ru isotopic ratios were corrected for mass fractionation using the deviation of the standard average run on the day over the natural ratio of the element. External reproducibility on HSE analyses was better than 0.5% for 5 ppb solutions and all reported values are blank corrected. Peridotite standard reference materials (MUH-1, HARZ-01) run during the period of the analytical campaign in the SIGL are reported in Day et al. (2016a) and Snortum & Day (2020) and show good reproducibility and accuracy compared with literature data (e.g., Meisel & Horan, 2016). The total procedural blanks (n = 4) run with the samples had $^{187}Os/^{188}Os = 0.209 \pm 0.090$, with quantities (in pg) of 0.8 [Re], 7 [Pd], 22 [Pt], 15 [Ru], 3 [Ir] and 0.8 [Os]. These blanks resulted in negligible corrections to samples (<1% in most cases, Table S3).

3. RESULTS

3.1. Sample descriptions and mineral chemistry

Spinel grains in the PAR abyssal peridotites from WEST03MV-12 and WEST03MV-13 span a Mg# range of 58.4 to 70.6 and 68.7 to 72.7, and a Cr# range of 28.7 to 49.6 and 19.1 to 24.9, respectively, similar to plagioclase-free peridotites (e.g., SWIR peridotites, Seyler et al., 2003; global abyssal peridotite database, Warren, 2016). Spinel grains in Hess Deep (EPR) samples have Mg# between 45.6 and 60.0, and Cr# between 47.3 and 52.0 (e.g., comparable to plagioclase-lherzolites from the SWIR; Paquet et al., 2016) (Fig. S1a).

Forsterite contents in olivine grains range between 89.7 and 90.7, and between 90.0 and 90.6 in WEST03MV-12 and WEST03MV-13 samples, respectively (Table S4). Orthopyroxenes and clinopyroxenes in PAR samples have similar compositions: between $Wo_{0.01\text{-}0.07}En_{0.84\text{-}0.89}Fs_{0.08\text{-}0.10}$ and $Wo_{0.32\text{-}0.49}En_{0.47\text{-}0.62}Fs_{0.05\text{-}0.07}$ for WEST03MV-12 peridotites, and between $Wo_{0.01\text{-}0.11}En_{0.81\text{-}0.89}Fs_{0.09\text{-}0.10}$ and $Wo_{0.35\text{-}0.49}En_{0.46\text{-}0.59}Fs_{0.04\text{-}0.06}$ for the WEST03MV-13 peridotites (Fig. S1b). WEST03MV-12 and WEST03MV-13 peridotites have Cr_2O_3 contents that range from 0.66 to 1.08 wt.% and from 0.43 to 0.96 wt.% in orthopyroxenes, and from 0.95 to 1.43 wt.% and from 0.56 to 1.32 wt.% in clinopyroxenes, respectively (Table S4). These values are within the compositions of abyssal peridotites from the global ridge system (e.g., Warren, 2016). Olivine, orthopyroxene and clinopyroxene grains in the EPR samples were not fresh enough to conduct analyses on.

3.2. Bulk rock major and trace element abundances

Hess Deep abyssal peridotites tend to have lower anhydrous-corrected Al_2O_3, TiO_2 and CaO, and higher MgO contents than to those from the Pacific Antarctic Ridge (Fig. 2, Table S5). The WEST03MV-13 peridotites generally have lower Al_2O_3, TiO_2 and CaO (and Fe_2O_{3T} to a lesser extent) at a given MgO than the WEST03MV-12 peridotites, suggesting heterogeneity at the scale of the fracture zone that they were dredged from. All these peridotites show a positive correlation between Al_2O_3 and CaO, with Hess Deep peridotites being both tightly grouped in terms of composition and having the most refractory (lowest) Al_2O_3 and CaO contents. Overall, the Pacific abyssal peridotites overlap the trend defined by abyssal peridotites from ridges with slower spreading rates (Day et al., 2017a).

Abyssal peridotites from the UFZ along the PAR are characterized by having subchondritic rare earth element (REE) abundances, and show pronounced LREE-depleted patterns, which are similar to abyssal peridotites from the Mid-Atlantic Ridge, and some samples from the SWIR and Gakkel Ridge (Day et al., 2017a) (Figs. 3, S2 and Table S6). Samples from the WEST03MV-12 dredge span a larger range of REE abundances. Abyssal peridotites from Hess Deep are depleted in the heavy REE, with REE patterns slightly depleted in the light REE (LREE) relative to the HREE, and strong positive anomalies for Eu, suggesting melt impregnation and plagioclase crystallization. A few samples from the PAR, SWIR and CIR also show negative Ce anomalies. Overall, abyssal peridotites from the WEST03MV-13 dredge tend to have higher Nb and Ta abundances, and lower Zr and Hf abundances than those from the WEST03MV-12 dredge. Abyssal peridotites from Hess Deep exhibit depleted patterns in Rb, Ba, Nb, Ta, Zr and Hf compared to other Pacific peridotites. In general, incompatible trace element (ITE) and

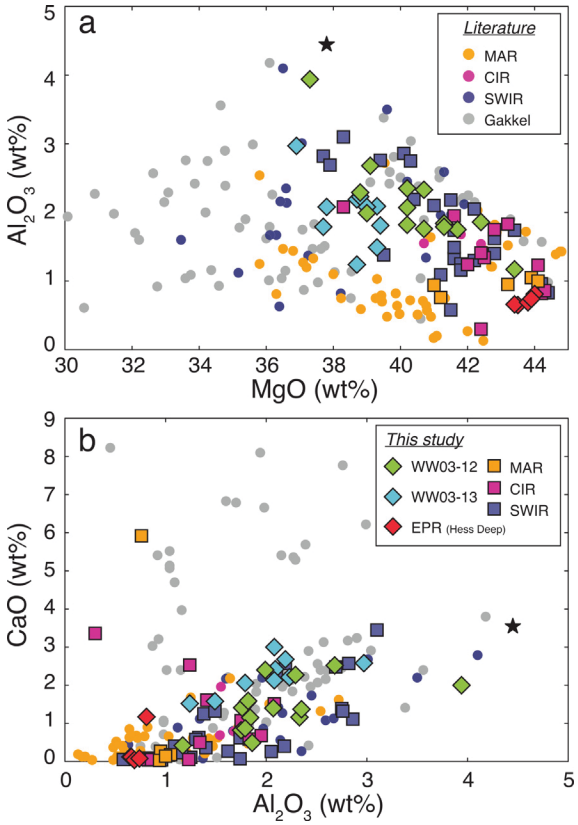

Fig. 2. Variations (in wt.%) of (a) Al_2O_3 as a function of MgO and (b) CaO as a function of Al_2O_3 for bulk rock abyssal peridotites from the dredges WEST03MV-12 and WEST03MV-13 (abbreviated WW03-12 and WW03-13, respectively) along the Pacific Antarctic Ridge, the Hess Deep region along the East Pacific Rise, the Southwest Indian Ridge, the Central Indian Ridge and the Mid-Atlantic Ridge. Also shown for comparison are abyssal peridotites from the Gakkel Ridge, the Southwest Indian Ridge, the Central Indian Ridge and the Mid-Atlantic Ridge for which HSE and Os isotope data are available (see Table S7 for references). The star corresponds to the Primitive Mantle estimate from McDonough & Sun (1995). (For interpretation of the references to color in this figure legend, the reader is referred to the web version of this article).

REE abundances for abyssal peridotites from the SWIR are in good agreement with data reported in previous studies (e.g., Day et al., 2017a) (Figs. 3, S2 and Table S6).

Abyssal peridotites from the CIR reported in this study show more depleted patterns in the REE, and for the ITE in general with lower Nb contents (and slightly higher Ta abundances), than previously reported samples (e.g., Day et al., 2017a). PLUM05 abyssal peridotite samples from the MAR have HREE similar to those from the same ocean basin in the literature but are more enriched in the LREE and have more pronounced positive Eu anomalies. They also exhibit higher contents in Rb, Ba, Nb and Ta, but lower Zr and Hf abundances than those from Day et al. (2017a). Most abyssal peridotites show elevated concentrations in fluid mobile elements such as U and Sr which are enriched in seawater (Fig. S2).

3.3. Highly siderophile element abundances and Os isotopic compositions

Bulk rock Re-Os isotope and HSE abundance measurements for Pacific abyssal peridotites and some Southwest Indian Ridge and Central Indian Ridge peridotites are reported in Table 1. PAR samples from the WEST03MV-13 dredge have BSE-like HSE patterns with variable rhenium depletion, whereas samples from the WEST03MV-12 dredge have more variable Re, Pd and Pt abundances (Fig. 4), similar to those reported previously (Roy-Barman and Allègre, 1994; Snow and Schmidt, 1998; Rehkämper et al., 1999). Two of the Hess Deep samples have patterns that are akin to BSE, while the other samples show variable degrees of rhenium depletion relative to BSE. WEST03MV-12 and WEST03MV-13 abyssal peridotites have average Pd/Ir ratios of 1.4 ± 0.6 and 1.4 ± 1.1 (2 SD), and average Ru/Ir ratios of 1.7 ± 0.2 and 1.8 ± 0.4, respectively (Fig. 5). Hess Deep samples show average ratios slightly higher but within uncertainties at 1.9 ± 1.1 and 2.0 ± 0.6 for Pd/Ir and Ru/Ir ratios, respectively. Moreover, HSE patterns for the Pacific abyssal peridotites are like those from the Mid-Atlantic Ridge, and some of the abyssal peridotites from the Southwest Indian Ridge (Day et al., 2017a and references therein).

Pacific Antarctic Ridge peridotites show similar ranges and averages in $^{187}Os/^{188}Os$ (WEST03MV-12: 0.1264 ± 0.0054; WEST03MV-13: 0.1272 ± 0.0082; all uncertainties are 2 SD), and are slightly more radiogenic, on average, than the samples from Hess Deep (0.1247 ± 0.0030) (Fig. 6), with an average value of 0.1264 ± 0.0063 for all Pacific abyssal peridotites from this study. Using the Os abundances in the samples to calculate a weighted mean, we obtained a $^{187}Os/^{188}Os$ ratio of 0.1263. These new data overlap the trend defined by abyssal peridotites from slower spreading ridges (Snow & Schmidt, 1998; Rehkämper et al., 1999; Luguet et al., 2001; Liu et al., 2009; Lassiter et al., 2014; Day et al., 2017a), but are generally more radiogenic than mantle peridotites obtained from Pacific Ocean Islands (Snortum et al., 2019), which offer an alternate view of the Pacific oceanic mantle lithosphere.

4. DISCUSSION

4.1. Alteration and melt infiltration

Most abyssal peridotites have experienced serpentinization (<400 °C) and/or seafloor weathering (~0°C) under both oxidizing and reducing conditions (e.g., Snow & Dick, 1995; Bach et al., 2004; Paulick et al., 2006; Klein et al., 2013; Malvoisin, 2015). Samples in this study exhibit evidence for secondary alteration, manifested as loss on ignition (LOI) values of between ~5 and 17%, reflecting the presence of serpentine and other alteration minerals. As noted for abyssal peridotites from a range of spreading ridge environments (Niu, 2004; Harvey et al., 2006; Day et al., 2017a), elevated concentrations of fluid mobile elements occur in many of the samples, consistent with modification by interaction with seawater (e.g., U, Sr, K, P, Na, LREE; e.g., Frisby et al., 2016). However, most major and

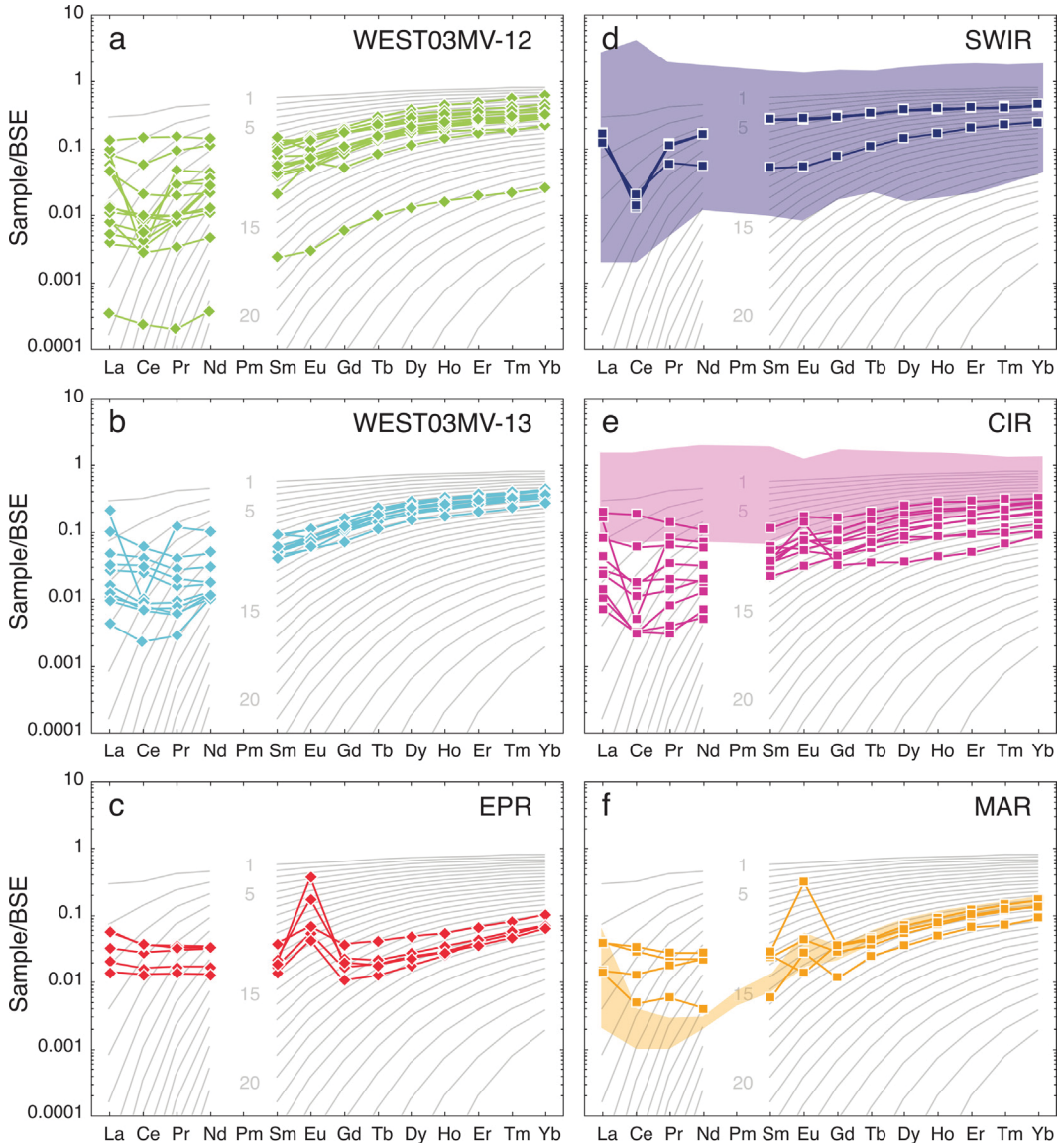

Fig. 3. Bulk Silicate Earth-normalized rare earth element (REE) concentrations in abyssal peridotites from the dredges WEST03MV-12 (a) and WEST03MV-13 (b) along the Pacific Antarctic Ridge (PAR), the Hess Deep region along the East Pacific Rise (EPR) (c), the SWIR (d), the CIR (e) and the MAR (f). Shaded fields are abyssal peridotites from Day et al., (2017a). Normalizing values from McDonough & Sun (1995). Gray lines represent 1% melt increments for a non-modal fractional melting model (see Day et al., 2017a for model parameters). An increase of melt depletion is associated with lower absolute REE abundances and higher depletion in the LREE relative to the HREE.

trace elements appear unaffected by alteration processes. Prior work has suggested that $^{187}Os/^{188}Os$ ratios (e.g., Snow & Reisberg, 1995; Standish et al., 2002), Re and Pd (e.g., Luguet et al., 2003; Harvey et al., 2006) can be modified by serpentinization and seafloor alteration processes but that, in general, abyssal peridotite HSE abundances are typically not strongly affected by such processes (e.g., Liu et al., 2009; Day et al., 2017a). In agreement with those studies, we find no correlation with LOI and HSE contents and Os isotopic compositions (Fig. S3). Indeed, it has been shown that even strongly steatized serpentinite rocks faithfully preserve original HSE abundances (Day et al., 2017b). Overall, we conclude that the bulk rock abyssal peridotite HSE compositions predominantly reflect their high temperature mantle petrogenesis.

Melt refertilization in abyssal peridotites (Niu, 2004; Seyler et al., 2004; Warren et al., 2009; Warren, 2016) can also lead to precipitation of metasomatic sulfides rich in Pd and the other HSE (Alard et al., 2000; Luguet et al., 2003). Evidence for melt refertilization in the sample suite is provided by the enrichments of non-fluid mobile highly incompatible elements in all samples (Fig. 3 and S2). Enrichments of two or three orders of magnitude in the high field strength elements (HFSE: Nb, Ta, Ti, Zr, Hf) relative to what would be expected for partial melting residues are strong indicators of melt refertilization in Pacific

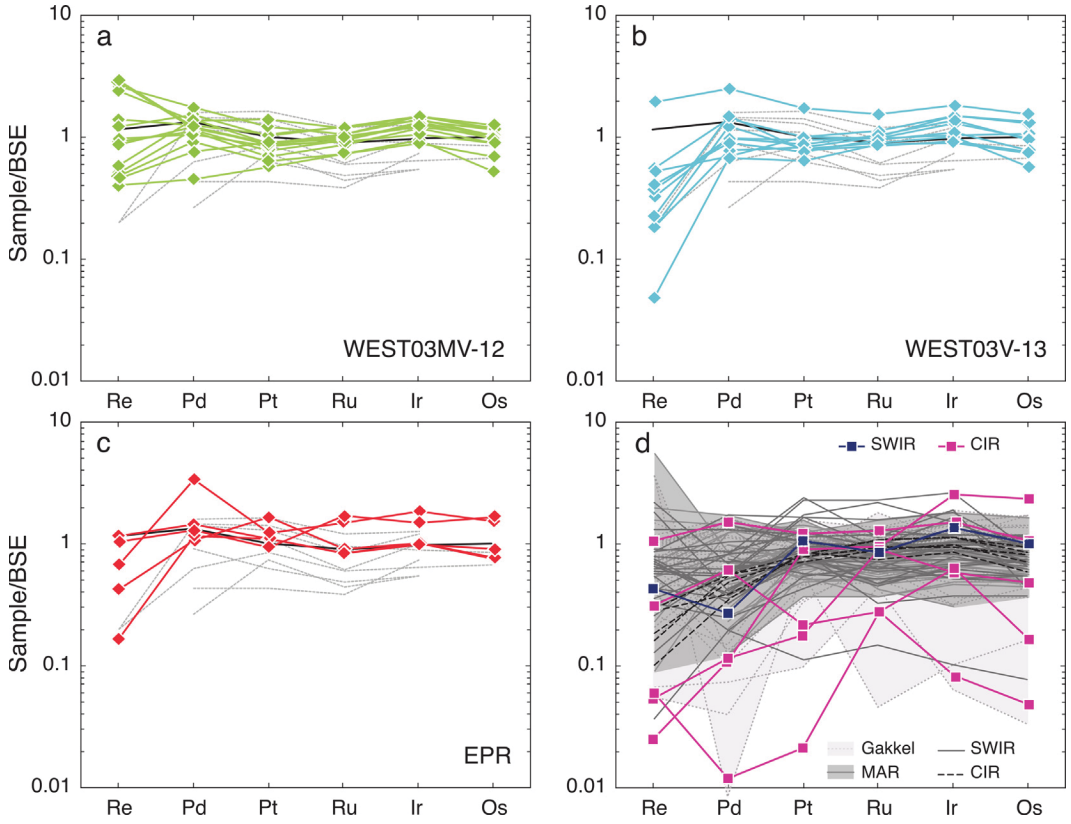

Fig. 4. Bulk Silicate Earth-normalized HSE concentrations in abyssal peridotites from the dredges WEST03MV-12 (a) and WEST03MV-13 (b) along the Pacific Antarctic Ridge (PAR), the Hess Deep region along the East Pacific Rise (EPR) (c), the SWIR and CIR, together with slow-spreading ridge abyssal peridotite literature data as comparison (Brandon et al., 2000: Liu et al., 2009; Lassiter et al., 2014; Day et al., 2017a; Li et al., 2019) (d). Normalizing values from Day et al. (2017a). Gray dashed lines (a-c) correspond to previous studies on Hess Deep abyssal peridotites (Snow & Schmidt, 1998; Rehkämper et al., 1999). The black solid line in panels a-c corresponds to the Primitive Upper Mantle (PUM) estimate from Becker et al. (2006).

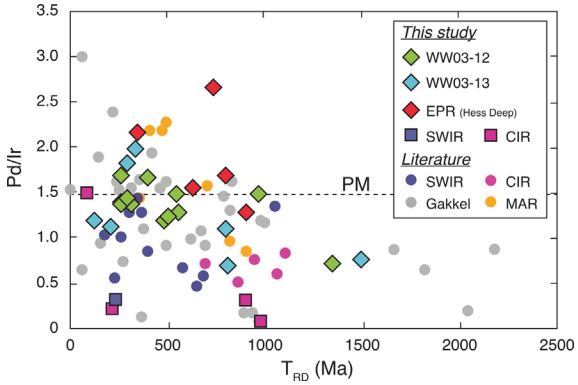

Fig. 5. Time of Re depletion model ages (T_{RD}) versus Pd/Ir. Primitive mantle (also referred to as BSE) Pd/Ir is from Day et al. (2017a). Literature data are from Snow and Schmidt (1998), Becker et al., 2006, Liu et al. (2008, 2009), and Day et al. (2017a). (For interpretation of the references to color in this figure legend, the reader is referred to the web version of this article).

abyssal peridotites (Fig. S2), along with some LREE-enriched peridotites, as observed in slower-spreading ridges (Niu et al., 2004; Warren, 2016; Day et al., 2017a). This melt infiltration has been variable between the sample suites, with plagioclase-rich melt infiltration possible in some sample suites (e.g., Hess Deep). These observations match with hand-specimen observations for AII125-6-4D-18, which include minor melt infiltration veins that are cross-cut by serpentine. Moreover, spinel grains in the Pacific abyssal peridotites plot within the lower part of the abyssal peridotite field, with relatively low Cr# at a given Mg#, which is often associated with the presence of pyroxenite-veins in the samples (e.g., Warren, 2016).

Melt infiltration events appear to have limited impact on Pt, Ru, Ir or Os abundances or Os isotopes in Pacific abyssal peridotites. In contrast, samples display variable Re contents, and Pd contents to a lesser extent (Fig. 4), which may be attributed to various degrees of refertilization by melts. As shown previously, basaltic melts typically have more radiogenic $^{187}Os/^{188}Os$ ratios, but substantially lower Os contents than peridotites, meaning that only high degrees of melt-rock reaction will lead to modification of peridotite HSE compositions (Day et al., 2017a). The generally high Os contents of the samples (~2–9 ppb) means that melt refertilization would only be notable at melt-rock ratios in excess of ten, which is not consistent with immobile incompatible trace element addition in all sam-

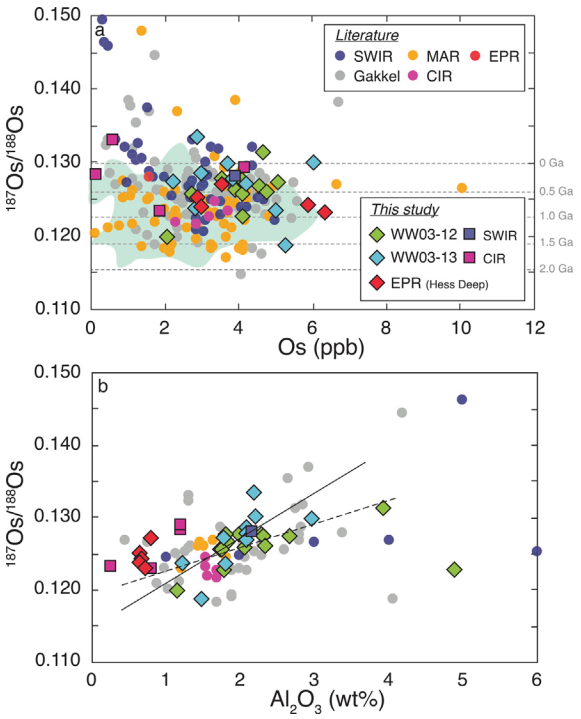

Fig. 6. Relationship between $^{187}Os/^{188}Os$ ratios and (a) Os and (b) Al_2O_3 contents in abyssal peridotites. The dashed and solid lines in (b) correspond to the linear regression for the WEST03MV-12 ($r^2 = 0.64$) and WEST03MV-13 peridotites ($r^2 = 0.5$), respectively. Literature data for abyssal peridotites are given in the text and can be found in Table S7. The green field represents the peridotite xenoliths from the Pacific Ocean (Bizimis et al., 2007; Jackson et al., 2016; Snortum et al., 2019). The dotted gray lines in (a) are the depletion ages for a BSE composition. (For interpretation of the references to color in this figure legend, the reader is referred to the web version of this article).

ples and suggests melt-rock ratios less than one. Even the peridotite with the lowest Os content in the sample set (CIRCE97-HD-2; 0.19 ppb Os) has a $^{187}Os/^{188}Os$ ratio within the range of the other peridotites, and distinct from more radiogenic MORB melts (e.g., Gannoun et al., 2016). These lines of evidence suggest that sulfide melt addition is not a significant driver in Pt, Ru, Ir or Os abundances or $^{187}Os/^{188}Os$ ratios in the studied abyssal peridotites. Conversely, melt refertilization can be pervasive and variable in extent from ultraslow to fast spreading ridges in modifying Re and Pd abundances (up to a factor 10 for Re abundances; Fig. 4).

4.2. Recent versus ancient processes acting on abyssal peridotites

Melt depletion processes can fundamentally modify peridotite compositions (e.g., Becker et al., 2006; Reisberg, 2021). It is possible to estimate the degree of melt depletion experienced by peridotites using a range of methods. For example, non-modal fractional melting models can be used to estimate melt depletion in abyssal peridotites based on REE abundances (here using model parameters outlined in Day et al., 2017a). An increase in melt depletion is associated with lower absolute REE abundances and higher depletion in the LREE relative to the HREE. The REE modeling calculations suggest 3–20% melt extraction for the WEST03MV-12 peridotites, 8–13% for the WEST03MV-13 peridotites, and 15–20% for the EPR peridotites. These estimates are consistent to slightly higher than calculations of melt depletion using Cr# in spinel grains from the same samples (e.g., Batanova et al., 1998; Hellebrand et al., 2001): 13.7–19.0%, 9.6–12.3% and 18.4–19.5%, respectively (Table S4). The more BSE-like HSE patterns in the WEST03MV-13 peridotites relate to more limited melt depletions than in other abyssal peridotite samples from the PAR and Hess Deep. The estimated high degrees of melt loss in some of the peridotites (WEST03MV-12 and Hess Deep) are consistent with clinopyroxene being nearly consumed within the mineral assemblage (Ol + Opx + Cpx + Sp) during partial melting. Correspondingly, melt extraction at fast-spreading ridges ranges up to higher values than those calculated for slow and ultraslow-spreading ridges (e.g., Warren, 2016; Day et al., 2017a) (Fig. S4).

Melt extraction in the mantle typically leads to the formation of residual peridotites depleted in Re, Pd ± Pt, relative to Ru, Ir and Os, reflecting the extraction of sulfide melt along with silicate melt, or dissolution of sulfides into the melt and formation of refractory platinum group minerals (e.g., Alard et al., 2000; Luguet et al., 2003; Ballhaus et al., 2006; Liu et al., 2009; Reisberg, 2021). Notably, Pacific abyssal peridotites tend to have BSE-like to fractionated HSE patterns with relative depletion in Re, Pd and Pt: all Pacific abyssal peridotites show similar ranges for $(Pd/Ir)_n$ and $(Pt/Ir)_n$ (WEST03MV-12 dredge: 0.5–1.2 and 0.6–0.9; WEST03MV-13 dredge: 0.5–1.6 and 0.5–1.0; EPR: 0.9–1.8 and 0.6–1.6, respectively). Pacific Antarctic Ridge samples with low degrees of melt depletion (WEST03MV-13) have BSE-like HSE patterns with variable rhenium depletion, whereas samples with higher degrees of melt depletion (WEST03MV-12) have more variable Re, Pd and Pt abundances (Fig. 4). Two of the Hess Deep samples have patterns that are akin to BSE, while the other samples show different degrees of rhenium depletion, suggesting that, in all cases, melt depletion has modified the original HSE abundances. The average total HSE content decreases with decreasing melt depletion degree (Fig. S5), suggesting that the variability observed between the different ocean basins in terms of HSE abundances can be explained by petrogenetic processes.

Melt depletion in peridotites decreases the incompatible element abundances. Positive correlations exist between Al_2O_3, as well as the HREE and Y, and $^{187}Os/^{188}Os$ ratios for the Pacific abyssal peridotites (Fig. 6), as observed for peridotites from slower spreading ridges (e.g., Reisberg and Lorand, 1995; Parkinson et al., 1998; Lassiter et al., 2014; Day et al., 2017a). Positive relationships also exist between Al_2O_3 and Re/Ir and Pd/Ir, but do not occur for Pt/Ir, Ru/Ir or Os/Ir, which are essentially invariant with decreasing Al_2O_3 (Table 1). Rhenium and Pd abundances in abyssal peridotites are depleted during melt loss, whereas Pt, Ru, Ir and Os abundances and $^{187}Os/^{188}Os$ ratios are less

affected by such processes. Consequently, these correlations reflect variable melt loss in the peridotite suite. The correlation between $^{187}Os/^{188}Os$ ratios and Al_2O_3 contents in bulk rock abyssal peridotites further implies that some of this melt depletion is also ancient, as $^{187}Os/^{188}Os$ in these rocks tracks long-term melt depletion, where rocks with low Al_2O_3 also have low $^{187}Re/^{188}Os$. Pre-existing heterogeneities in peridotites have been noted in previous ^{187}Re-^{187}Os studies, reporting Re depletion ages ($T_{RD} = 1/1.67 \times 10^{-11} \times \ln\{[(0.127 - {}^{187}Os/^{188}Os_{sample})/0.40186] + 1\}$; where T_{RD} ages represent minimum depletion ages, assuming no ingrowth from ^{187}Re in abyssal peridotites since melt depletion) as ancient as 2 Ga for abyssal peridotites (e.g., Harvey et al., 2006; Liu et al., 2008; Lassiter et al., 2014; Day et al., 2017a), as well as for ophiolite peridotites (e.g., Büchl et al., 2004; Schulte et al., 2009; O'Driscoll et al., 2012, 2015) and mantle peridotites from ocean islands (Snortum et al., 2019). In this respect, it is notable that the concept of the T_{RD} model age was originally developed for highly refractory cratonic peridotites, where the estimated degree of melt extraction is ~30 to 50%, leading to nearly Re-free peridotitic residues (Walker et al., 1989; Luguet and Pearson, 2019; Reisberg, 2021, and references therein). Nonetheless, measured $^{187}Os/^{188}Os$ below the BSE or even chondritic values in mantle peridotites must reflect long-term rhenium depletion.

Rhenium depletion ages for Pacific abyssal peridotites range up to 1.3 Ga for peridotites from the WEST03MV-12 dredge, up to 1.5 Ga for those from the WEST03MV-13 dredge, and up to 0.9 Ga for Hess Deep (Fig. 5). The oldest rhenium depletion ages are therefore in the samples with the lowest degrees of melt depletion. The average Re depletion ages are 0.5 ± 0.3 Ga, 0.6 ± 0.5 Ga and 0.7 ± 0.2 Ga respectively, which are similar to previous estimates from abyssal peridotites (Lassiter et al., 2014; Day et al., 2017a). The distinction between ancient melt depletion and recent melt depletion at the ridge remains one of the most challenging issues to deconvolve in abyssal peridotites. No correlations between $^{187}Os/^{188}Os$ ratios or T_{RD} ages with degree of partial melting (or melt depletion, F) are observed, suggesting that separating pre-existing melt depletion from recent-ridge melt depletion cannot be directly established. Nevertheless, Pacific abyssal peridotites with low Pd/Ir also show ancient T_{RD} ages, similar to samples from slower spreading ridges (e.g., Lassiter et al., 2014; Day et al., 2017a), indicating that abyssal peridotites preserve significant pre-existing melt depletion, up to or exceeding 2 Ga, in some cases (Fig. 5).

4.3. Pacific Ocean mantle composition

Collectively, Pacific abyssal peridotites have similar distributions and variations in the abundances of the HSE, as well as slightly more radiogenic $^{187}Os/^{188}Os$, relative to Pacific mantle xenoliths (Fig. 6a) (Bizimis et al., 2007; Jackson et al., 2016; Snortum et al., 2019). Mantle xenoliths preserve melt depletion ages up to 1.5 Ga in Aitutaki (Cook Islands: Snortum et al., 2019), 1.5 Ga in Savai'i, 1.8 Ga in Tubuai (Samoa and Austral Islands, respectively: Jackson et al., 2016) and as ancient as 2 Ga in O'ahu (Hawaii: Bizimis et al., 2007), similar to T_{RD} ages reported for Pacific abyssal peridotites. These observations indicate that the Pacific oceanic mantle records heterogeneous melt-depletion from both ancient and more recent melt depletion events. These melt depletion events can be up to 2 Ga and, in this sense, are similar to observations from global oceanic lithosphere (e.g., Brandon et al., 2000; Harvey et al., 2006; Liu et al., 2008, 2009; Lassiter et al., 2014; Day et al., 2017a). Even though Pacific abyssal peridotites and mantle xenoliths only provide a glimpse of the Pacific oceanic plate, often at the hand-sample scale, they show evidence for significant heterogeneities at short length scales due to prior melt depletion events up to 2 Ga ago, as well as strong similarities in average HSE abundances and Os isotope compositions to abyssal peridotites from the Atlantic, Indian or Arctic Ocean basins.

4.4. Composition of the Bulk Silicate Earth deduced from abyssal peridotites

Average HSE abundances and Os isotope compositions for measured abyssal peridotites from the global mid-ocean ridge system show no correlation with spreading rate (Figs. 7 and S6). This observation is important because different melting processes at slow and ultraslow spreading ridges versus fast spreading ridges could conceivably yield differences in modern melt depletion recorded in abyssal peridotites, but this is not the case. The $^{187}Os/^{188}Os$ composition of the BSE recalculated with the new Pacific abyssal peridotites is 0.1265 ± 0.0031 (n = 230), and 0.1250 ± 0.0040 for peridotites with > 2 ppb Os. These values are close to those reported by Lassiter et al. (2014) for the convecting upper mantle and by Day et al. (2017a) for the depleted MORB mantle (0.1245 and 0.1247 ± 0.0075, respectively). Following a similar approach as Day et al. (2017a), we recalculate the average composition of the BSE using abyssal peridotites with Al_2O_3 content > 2 wt.% from all mid-ocean ridge systems (Fig. 8). We obtain 0.34 ± 0.38 (1 s.d.) ppb [Re], 4.87 ± 2.67 ppb [Pd], 7.29 ± 1.88 ppb [Pt], 7.40 ± 1.89 ppb [Ru], 3.84 ± 1.12 ppb [Ir] and 3.36 ± 1.09 ppb [Os] (Fig. 8). Estimates for the Arctic and Indian Oceans give comparable values to those of the global ridge system estimate (Fig. 8). Note that the Atlantic Ocean estimate appears slightly depleted, and the Pacific Ocean is slightly enriched in HSE, compared with the global BSE estimate (Fig. 8). These differences can be attributed to variable degrees of ancient and modern partial melting affecting the peridotites. Similar results are obtained when the data are regressed to a BSE Al_2O_3 value of 4 to 4.5 wt.% (see Day et al., 2017a).

The reevaluated composition for the BSE, including the new Pacific abyssal peridotite data, does not significantly change the average estimates for the BSE previously reported for abyssal and oceanic peridotites (Becker et al., 2006; Chatterjee and Lassiter, 2016; Day et al., 2017a), or for continental peridotites (Becker et al., 2006; Chatterjee and Lassiter, 2016). Our results for Pacific abyssal peridotites confirm that the BSE estimated from abyssal peridotites does not show high Pd/Ir and Pd enrichment as reported by Becker et al. (2006), and Chatterjee and

Lassiter (2016). This discrepancy between the two estimates of the BSE composition is thought to result from Pd enrichment in the continental-derived peridotites used for the calculation due to melt-refertilization (e.g., Aulbach et al., 2016; Luguet and Reisberg, 2016; Becker and Dale, 2016). Overall, these observations lead to the idea that the BSE shows an abundance range for the most incompatible HSE (Re, Pd) that can exceed one hundred percent, but that more compatible HSE (Pt, Ru, Ir, Os) show less than 30% abundance variation. These variations can be accounted for by melting processes acting on abyssal peridotites over < 2 Ga.

4.5. Implications of a relatively homogeneous convecting mantle for the HSE

Abyssal peridotites from fast to intermediate spreading ridges reveal few, if any, systematic differences in the distribution and behavior of the HSE, compared with slow to ultraslow spreading ridges, despite generally higher degrees of melt depletion (Figs. 7 and 8). Additionally, estimates of the $^{187}Os/^{188}Os$ isotope composition of the BSE based on abyssal peridotites show little to no difference to oceanic mantle xenoliths (e.g., Chatterjee and Lassiter, 2016; Snortum et al., 2019) and samples from peridotite massifs (e.g., Becker et al., 2006). Taking the available global abyssal peridotite sample set and using Al_2O_3 > 2 wt.%, HSE and Os isotope compositions argue in favor of present-day convecting mantle composition, with Pt, Ru, Ir and Os abundance variations at <±30% and $^{187}Os/^{188}Os$ variations at ~6% (2SD) for the global abyssal peridotite dataset. As noted previously, this variation can be accounted for by recent rather than ancient (>2 Ga) processes.

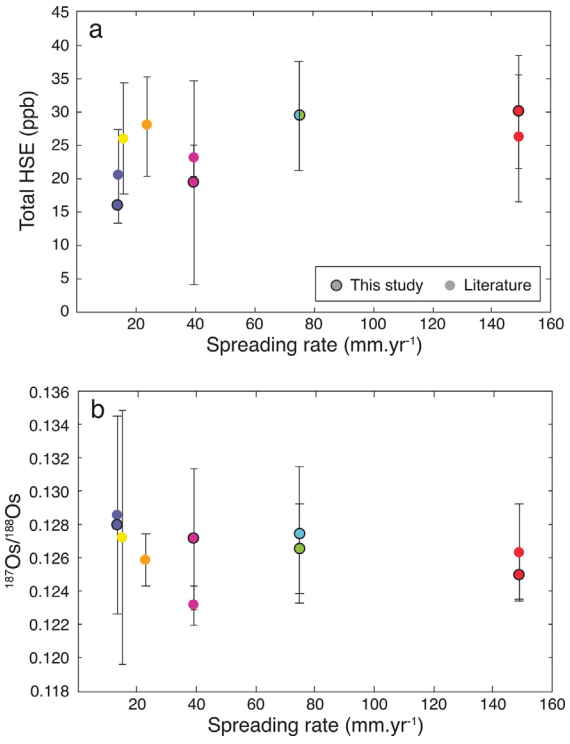

Fig. 7. Average (a) total HSE contents in ppb, and (b) $^{187}Os/^{188}Os$ ratios as a function of spreading rate. Spreading rates are as reported in Fig. 1.

Compared with abyssal peridotites (e.g., Day et al., 2017a and this study), Archean mantle peridotites from West Greenland (3.8 Ga) and Western Australia (3.46 Ga) have similar broadly chondritic $^{187}Os/^{188}Os$ compositions and Os concentrations, arguing in favor of the HSE being added to the Earth, transported and homogenized within the mantle by ~3.8 Ga (Bennett et al., 2002; van de Löcht et al., 2018). Homogeneous Ru isotope compositions have been reported in Archean ultramafic rocks younger than 3.5 Ga (Pilbara Craton, Australia: 3.5–3.2 Ga; Abitibi greenstone belt, Canada: 2.7 Ga; Bushveld, South Africa: 2.05 Ga), as well as in Phanerozoic oceanic and continental mantle domains, and are undistinguishable from the modern terrestrial mantle (Bermingham and Walker, 2017; Fischer-Gödde et al., 2020). These lines of evidence all support a relatively homogenized BSE in terms of HSE abundances and Os isotope ratios since at least the Archaean, where variations reflect melting processes within the mantle, rather than heterogeneities incorporated during Earth's accretion.

Based on HSE abundances, it has been proposed that ~0.5 to 0.8% of Earth's present mass was accreted after core formation, if all HSE delivered by these impacts were retained in the mantle, rather than being lost to the core or through inefficient impact retention (Becker et al., 2006; Day et al., 2016a). Consequently, late accretion impacts might have been expected to leave graininess in HSE abundances in Earth's mantle. This is because some moderate to large size impactors may not have been capable of completely remelting Earth's mantle. From a geological perspective, Eoarchean ultramafic rocks from Greenland (3.8–3.7 Ga), and Mesoarchean chromitites from Seqi, Greenland (minimum age of 3 Ga) exhibit ^{100}Ru excess (Fischer-Gödde et al., 2020), arguing in favor of a heterogeneous delivery of the HSE to the Earth during late accretion. Similarly, evidence for grainy accretion has been suggested for other bodies, such as Vesta (Day et al., 2012). Numerical impact models also support that delivery of silicate and metal to the Earth by large planetesimals was heterogeneous, leading to projectile material being concentrated within localized domains of Earth's mantle and producing isotopic anomalies in W, Mo and Ru isotopes (Marchi et al., 2018; Maas et al., 2021).

Geochemical arguments in favor of heterogeneities imparted to the mantle during accretion include positive $\mu^{182}W$ preserved in most Eoarchean rocks studied to date, which have been interpreted to indicate that late accreted materials were not evenly distributed in Earth's mantle, and not well mixed in the BSE (Willbold et al., 2011). Such heterogeneities are not evident in the convecting mantle, with basalts from mid-ocean ridges and ocean islands measured to date lacking positive $\mu^{182}W$ anomalies (e.g., Mundl et al., 2017). The HSE have also been argued to have been heterogeneously distributed within the early mantle from observations that Archean (3.5–3.2 Ga) komatiites from the Barberton greenstone belt (South Africa) and

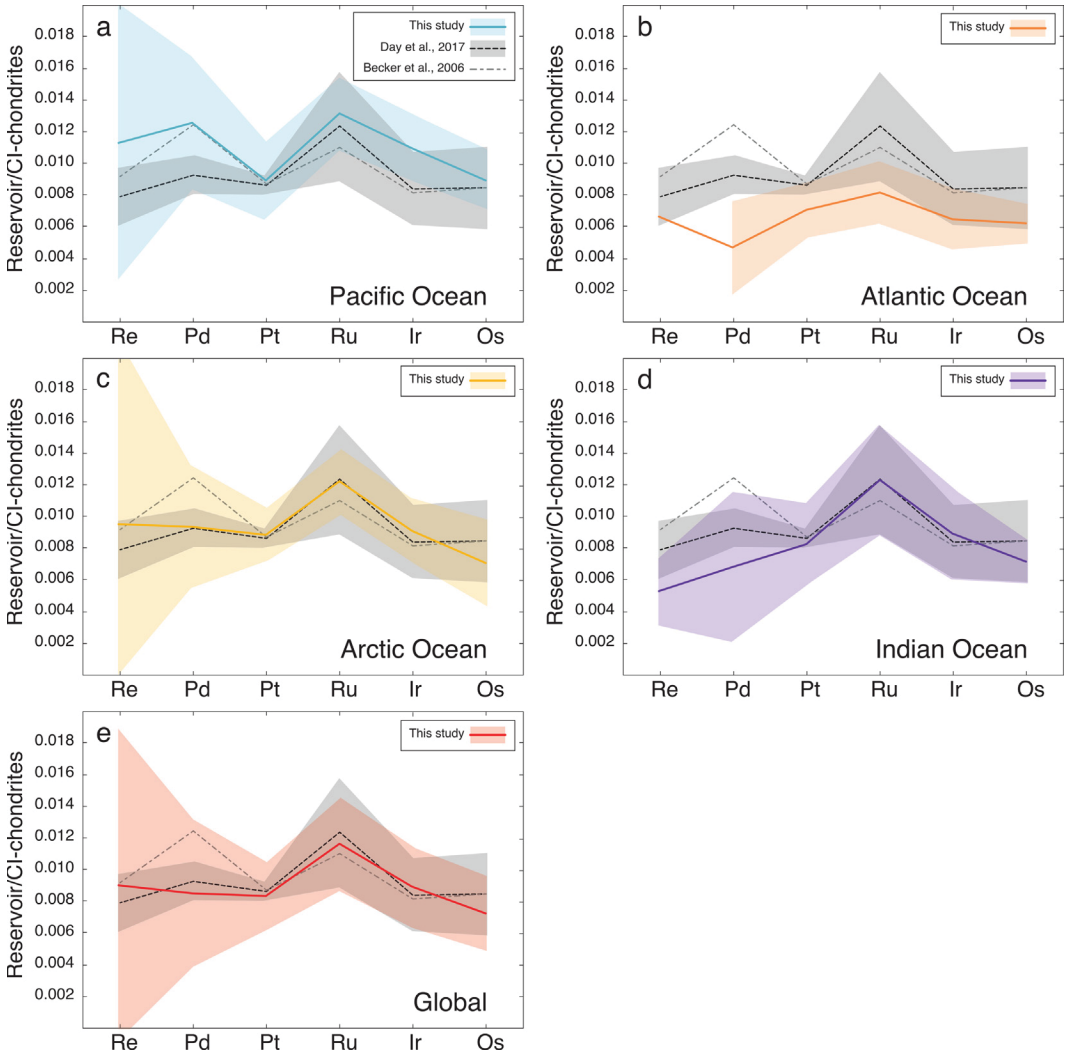

Fig. 8. Estimates for the mantle composition for each ocean basin (solid lines), considered to be represented by abyssal peridotites with $Al_2O_3 > 2$ wt.% (this study; Brandon et al., 2000: Liu et al., 2009; Lassiter et al., 2014; Day et al., 2017a; Li et al., 2019) (a) Pacific Ocean, (b) Atlantic Ocean, (c) Arctic Ocean, (d) Indian Ocean and (e) for the global abyssal peridotite sample suite. Colored fields correspond to the standard deviation of the calculated mantle composition. Dashed lines correspond to the primitive (upper) mantle estimates from Becker et al., (2006) and Day et al. (2017a). The gray field represents the 2 SD uncertainty of the estimate from Day et al. (2017a). Note that abyssal peridotites from the CIR and Hess Deep along the EPR were not included in the calculation for the Indian and Pacific oceans due to their low Al_2O_3 content. (For interpretation of the references to color in this figure legend, the reader is referred to the web version of this article).

the Pilbara craton (Western Australia) apparently record depleted HSE compositions for their mantle sources relative to late Archean and younger komatiites (Maier et al., 2009). Arguments in favor of HSE heterogeneities imparted to the mantle by late accretion are not without controversy, however, where it has been argued that komatiites are not faithful recorders of mantle source compositions (Waterton et al., 2021).

Because the HSE appear to be homogeneously mixed in the present-day convecting mantle, we favor that whatever HSE input was accreted to the Earth, these heterogeneities have been relatively efficiently mixed into the mantle through convective processes. Anomalies in the HSE, including Ru, as well as Mo and W in Archean crustal rocks can be interpreted to reflect late accretion heterogeneity within the Earth that is well-recorded within isolated crustal and lithospheric fragments. For example, the mantle beneath southwest Greenland had not yet fully equilibrated with late accretion material by 3.7 Ga ago (Fischer-Gödde et al., 2020). This is consistent with the average mantle homogenization timescale of ~1.2 Ga calculated from the combined $^{186}Os/^{188}Os$-$^{187}Os/^{188}Os$ isotopic and Pt/Os and Re/Os variability in peridotites (e.g., Chatterjee and Lassiter, 2016). Other isotopic systems, such as the short lived ^{146}Sm-^{142}Nd system, lead to younger mantle homogenization timescales (~0.4 Ga) as well as a fast mantle stirring rate (e.g., Chatterjee and Lassiter, 2016; Hyung and Jacobsen, 2020).

In contrast with lithophile incompatible elements, which are sensitive to resetting by melt refertilization in peridotites, the Re-Os and Pt-Os isotope systems are less susceptible to similar petrogenetic processes. As such, the

mixing timescale inferred from Os isotopes in abyssal peridotites of around 0.5–0.7 Ga is approximately consistent with timescales predicted for the whole mantle convection. Hoffman and McKenzie (1985) showed that any convecting region of the upper mantle will be well mixed on a horizontal scale of at least 2000 km in 400 Ma, or 8500 km in 1.5 Ga, suggesting that large scale heterogeneities would be destroyed within Earth's lifetime. Our data support this contention. Nonetheless, elemental and isotopic anomalies that are thought to reflect mantle heterogeneities have been recorded in ocean island basalts (e.g., HSE in the Réunion cumulate xenoliths, Peters et al., 2016; W isotope anomalies in modern flood basalts: Rizo et al., 2016; and modern ocean island basalts: Mundl et al., 2017; Mundl-Petermeier et al., 2019, 2020; Peters et al., 2021). These suggest that distinct mantle domains might have been effectively isolated and preserved from the convecting upper mantle through most of the Earth's history (e.g., Allègre and Turcotte, 1985).

5. CONCLUSIONS

This global survey of abyssal peridotites from fast to intermediate spreading ridges reveals few if any systematic differences in the distribution and behavior of the HSE, compared with slow to ultraslow spreading ridges, despite variable degrees of melt depletion. Melt refertilization is pervasive and variable in extent from ultraslow to fast spreading ridges and can modify Re and Pd quite significantly. Across ocean basins and independently of spreading rates, the HSE appear relatively homogeneous in the BSE. Using abyssal peridotites with Al_2O_3 content > 2 wt.% from all mid-ocean ridge systems, including the new Pacific abyssal peridotite data, we recalculated the average composition of the BSE of 0.30 ± 0.33 ppb [Re], 4.94 ± 2.35 ppb [Pd], 7.13 ± 2.16 ppb [Pt], 7.22 ± 3.71 ppb [Ru], 3.79 ± 1.84 ppb [Ir] and 3.77 ± 1.45 ppb [Os]. Variability observed between the different ocean basins, if any, can most likely be explained by partial melting processes. The variations in HSE abundances currently observed within the convecting mantle sampled by abyssal peridotites are primarily due to partial melting and melt refertilization processes over the past 2 Ga rather than to significant HSE heterogeneity of the post-Archean mantle. Preservation of ancient melt depletion heterogeneities in some oceanic peridotites, with osmium T_{RD} ages exceeding 1 Ga and highly depleted Hf isotope signatures measured in clinopyroxene grains (Stracke et al., 2011; Sanfilippo et al., 2019) suggests some refractory domains formed through ancient melt depletion can also be partially preserved in the convecting upper mantle.

Declaration of Competing Interest

The authors declare that they have no known competing financial interests or personal relationships that could have appeared to influence the work reported in this paper.

ACKNOWLEDGEMENTS

This work was largely supported by a University of California San Diego Academic Senate Award, and in part, by the NSF Petrology and Geochemistry program (NSF EAR 1447130 and EAR 1918322 to JMDD). We are grateful to Alex Hangsterfer (SIO Geological Collections) for assistance with sample curation. Dean Poeppe and Garrett Stewart are thanked for assistance with sample preparation. Constructive comments from David van Acken, the Associate Editor, Andreas Stracke, and two anonymous reviewers are gratefully acknowledged.

APPENDIX A. SUPPLEMENTARY MATERIAL

Supplementary data to this article can be found online at https://doi.org/10.1016/j.gca.2021.09.033.

REFERENCES

Alard O., Luguet A., Pearson N. J., Griffin W. L., Lorand J. P., Gannoun A. and O'Reilly S. Y. (2005) In situ Os isotopes in abyssal peridotites bridge the isotopic gap between MORBs and their source mantle. *Nature* **436**(7053), 1005–1008.

Alard O., Griffin W. L., Lorand J. P., Jackson S. E. and O'Reilly S. Y. (2000) Non-chondritic distribution of the highly siderophile elements in mantle sulphides. *Nature* **407**, 891–894.

Allègre C. J. and Turcotte D. L. (1985) Geodynamic mixing in the mesosphere boundary layer and the origin of oceanic islands. *Geophys. Res. Lett.* **12**(4), 207–210.

Aulbach S., Mungall J. E. and Pearson D. G. (2016) Distribution and processing of highly siderophile elements in cratonic mantle lithosphere. *Rev. Mineral. Geochem.* **81**(1), 239–304.

Bach W., Garrido C. J., Paulick H., Harvey J. and Rosner M. (2004) Seawater-peridotite interactions: First insights from ODP Leg 209, MAR 15°N. *Geochem. Geophys. Geosyst.* **5**(9).

Ballhaus C., Bockrath C., Wohlgemuth-Ueberwasser C., Laurenz V. and Berndt J. (2006) Fractionation of the noble metals by physical processes. *Contrib. Miner. Petrol.* **152**(6), 667–684.

Batanova V. G., Suhr G. and Sobolev A. V. (1998) Origin of geochemical heterogeneity in the mantle peridotites from the Bay of Islands ophiolite, Newfoundland, Canada: ion probe study of clinopyroxenes. *Geochim. Cosmochim. Acta* **62**(5), 853–866.

Becker H. and Dale C. W. (2016) Re–Pt–Os isotopic and highly siderophile element behavior in oceanic and continental mantle tectonites. *Rev. Mineral. Geochem.* **81**(1), 369–440.

Becker H., Horan M. F., Walker R. J., Gao S., Lorand J. P. and Rudnick R. L. (2006) Highly siderophile element composition of the Earth's primitive upper mantle: constraints from new data on peridotite massifs and xenoliths. *Geochim. Cosmochim. Acta* **70**(17), 4528–4550.

Bennett V. C., Nutman A. P. and Esat T. M. (2002) Constraints on mantle evolution from $^{187}Os/^{188}Os$ isotopic compositions of Archean ultramafic rocks from southern West Greenland (3.8 Ga) and Western Australia (3.46 Ga). *Geochim. Cosmochim. Acta* **66**(14), 2615–2630.

Birck J. L., Barman M. R. and Capmas F. (1997) Re-Os isotopic measurements at the femtomole level in natural samples. *Geostandards Newsletter* **21**(1), 19–27.

Bermingham K. R. and Walker R. J. (2017) The ruthenium isotopic composition of the oceanic mantle. *Earth Planet. Sci. Lett.* **474**, 466–473.

Bizimis M., Griselin M., Lassiter J. C., Salters V. J. and Sen G. (2007) Ancient recycled mantle lithosphere in the Hawaiian plume: osmium–hafnium isotopic evidence from peridotite mantle xenoliths. *Earth Planet. Sci. Lett.* **257**(1–2), 259–273.

Bottke W. F., Walker R. J., Day J. M. D., Nesvorny D. and Elkins-Tanton L. (2010) Stochastic late accretion to Earth, the Moon, and Mars. *Science* **330**(6010), 1527–1530.

Brandon A. D., Snow J. E., Walker R. J., Morgan J. W. and Mock T. D. (2000) ^{190}Pt-^{186}Os and ^{187}Re-^{187}Os systematics of abyssal peridotites. *Earth Planet. Sci. Lett.* **177**, 319–335.

Brandon A. D., Walker R. J. and Puchtel I. S. (2006) Platinum–osmium isotope evolution of the Earth's mantle: constraints from chondrites and Os-rich alloys. *Geochimica et Cosmochimica Acta* **70**(8), 2093–2103.

Brenan J. M., Bennett N. R. and Zajacz Z. (2016) Experimental results on fractionation of the highly siderophile elements (HSE) at variable pressures and temperatures during planetary and magmatic differentiation. *Rev. Mineral. Geochem.* **81**(1), 1–87.

Brenan J. M. and McDonough W. F. (2009) Core formation and metal–silicate fractionation of osmium and iridium from gold. *Nat. Geosci.* **2**(11), 798.

Büchl A., Brügmann G. and Batanova V. G. (2004) Formation of podiform chromitite deposits: implications from PGE abundances and Os isotopic compositions of chromites from the Troodos complex, Cyprus. *Chem. Geol.* **208**(1–4), 217–232.

Castillo P. R., Natland J. H., Niu Y. and Lonsdale P. F. (1998) Sr, Nd and Pb isotopic variation along the Pacific-Antarctic risecrest, 53–57°S: implications for the composition and dynamics of the South Pacific upper mantle. *Earth Planet. Sci. Lett.* **154**(1–4), 109–125.

Chatterjee R. and Lassiter J. C. (2016) ^{186}Os/^{188}Os variations in upper mantle peridotites: Constraints on the Pt/Os ratio of primitive upper mantle, and implications for late veneer accretion and mantle mixing timescales. *Chem. Geol.* **442**, 11–22.

Chou, C. L. (1978). Fractionation of siderophile elements in the Earth's upper mantle. In Lunar and Planetary Science Conference Proceedings (Vol. 9).

Cohen A. S. and Waters F. G. (1996) Separation of osmium from geological materials by solvent extraction for analysis by thermal ionisation mass spectrometry. *Anal. Chim. Acta* **332**(2–3), 269–275.

Day J. M. D., O'Driscoll B., Strachan R. A., Daly J. S. and Walker R. J. (2017a) Identification of mantle peridotite as a possible Iapetan ophiolite sliver in south Shetland, Scottish Caledonides. *J. Geol. Soc. London* **174**, 88–92.

Day J. M. D., Walker R. J. and Warren J. M. (2017b) ^{186}Os–^{187}Os and highly siderophile element abundance systematics of the mantle revealed by abyssal peridotites and Os-rich alloys. *Geochim. Cosmochim. Acta* **200**, 232–254.

Day J. M. D., Waters C. L., Schaefer B. F., Walker R. J. and Turner S. (2016a) Use of hydrofluoric acid desilicification in the determination of highly siderophile element abundances and Re-Pt-Os isotope systematics in mafic-ultramafic rocks. *Geostand. Geoanal. Res.* **40**(1), 49–65.

Day J. M. D., Brandon A. D. and Walker R. J. (2016b) Highly siderophile elements in Earth, Mars, the Moon, and asteroids. *Rev. Mineral. Geochem.* **81**(1), 161–238.

Day J. M. D., Peters B. J. and Janney P. E. (2014) Oxygen isotope systematics of South African olivine melilitites and implications for HIMU mantle reservoirs. *Lithos* **202**, 76–84.

Day J. M. D., Walker R. J., Qin L. and Rumble, III, D. (2012) Late accretion as a natural consequence of planetary growth. *Nat. Geosci.* **5**(9), 614–617.

DeMets C., Gordon R. G., Argus D. F. and Stein S. (1990) Current plate motions. *Geophys. J. Int.* **101**(2), 425–478.

Ertel W., O'Neill H. S. C., Sylvester P. J., Dingwell D. B. and Spettel B. (2001) The solubility of rhenium in silicate melts: implications for the geochemical properties of rhenium at high temperatures. *Geochim. Cosmochim. Acta* **65**(13), 2161–2170.

Fischer-Gödde M., Elfers B. M., Münker C., Szilas K., Maier W. D., Messling N., Morishita T., Van Kranendonk M. and Smithies H. (2020) Ruthenium isotope vestige of Earth's pre-late-veneer mantle preserved in Archaean rocks. *Nature* **579**(7798), 240–244.

Fischer-Gödde M., Becker H. and Wombacher F. (2011) Rhodium, gold and other highly siderophile elements in orogenic peridotites and peridotite xenoliths. *Chem. Geol.* **280**(3–4), 365–383.

Frisby C., Bizimis M. and Mallick S. (2016) Seawater-derived rare earth element addition to abyssal peridotites during serpentinization. *Lithos* **248**, 432–454.

Gannoun A., Burton K. W., Day J. M. D., Harvey J., Schiano P. and Parkinson I. (2016) Highly siderophile element and Os Isotope Systematics of volcanic rocks at divergent and convergent plate boundaries and in intraplate settings. *Rev. Mineral. Geochem.* **81**, 651–724.

Haller M. B., O'Driscoll B., Day J. M. D., Daly J. S., Piccoli P. M. and Walker R. J. (2021) Meter-Scale Chemical and Isotopic Heterogeneities in the Oceanic Mantle, Leka Ophiolite Complex, Norway in press. *J. Petrology*.

Harvey J., Gannoun A., Burton K. W., Rogers N. W., Alard O. and Parkinson I. J. (2006) Ancient melt extraction from the oceanic upper mantle revealed by Re–Os isotopes in abyssal peridotites from the Mid-Atlantic ridge. *Earth Planet. Sci. Lett.* **244**(3–4), 606–621.

Hellebrand E., Snow J. E., Dick H. J. and Hofmann A. W. (2001) Coupled major and trace elements as indicators of the extent of melting in mid-ocean-ridge peridotites. *Nature* **410**(6829), 677–681.

Hoffman N. R. A. and McKenzie D. P. (1985) The destruction of geochemical heterogeneities by differential fluid motions during mantle convection. *Geophys. J. Int.* **82**(2), 163–206.

Holzheid A., Sylvester P., O'Neill H. S. C., Rubie D. C. and Palme H. (2000) Evidence for a late chondritic veneer in the Earth's mantle from high-pressure partitioning of palladium and platinum. *Nature* **406**(6794), 396–399.

Hyung E. and Jacobsen S. B. (2020) The ^{142}Nd/^{144}Nd variations in mantle-derived rocks provide constraints on the stirring rate of the mantle from the Hadean to the present. *Proc. Natl. Acad. Sci.* **117**(26), 14738–14744.

Jackson M. G., Shirey S. B., Hauri E. H., Kurz M. D. and Rizo H. (2016) Peridotite xenoliths from the Polynesian Austral and Samoa hotspots: Implications for the destruction of ancient ^{187}Os and ^{142}Nd isotopic domains and the preservation of Hadean ^{129}Xe in the modern convecting mantle. *Geochim. Cosmochim. Acta* **185**, 21–43.

Jagoutz, E., Palme, H., Baddenhausen, H., Blum, K., Cendales, M., Dreibus, G., Spettel, B., Lorenz, V. & Wänke, H. (1979). The abundances of major, minor and trace elements in the earth's mantle as derived from primitive ultramafic nodules. In Lunar and Planetary Science Conference Proceedings (Vol. 10, pp. 2031–2050).

Jones J. H. and Drake M. J. (1986) Geochemical constraints on core formation in the Earth. *Nature* **322**(6076), 221–228.

Kimura K. A. N., Lewis R. S. and Anders E. (1974) Distribution of gold and rhenium between nickel-iron and silicate melts: implications for the abundance of siderophile elements on the Earth and Moon. *Geochim. Cosmochim. Acta* **38**(5), 683–701.

Klein F., Bach W. and McCollom T. M. (2013) Compositional controls on hydrogen generation during serpentinization of ultramafic rocks. *Lithos* **178**, 55–69.

Lassiter J. C., Byerly B. L., Snow J. E. and Hellebrand E. (2014) Constraints from Os-isotope variations on the origin of Lena Trough abyssal peridotites and implications for the composition and evolution of the depleted upper mantle. *Earth Planet. Sci. Lett.* **403**, 178–187.

Li W., Liu C., Tao C. and Jin Z. (2019) Osmium isotope compositions and highly siderophile element abundances in abyssal peridotites from the Southwest Indian Ridge: Implications for evolution of the oceanic upper mantle. *Lithos* **346** 105167.

Liu C. Z., Snow J. E., Brügmann G., Hellebrand E. and Hofmann A. W. (2009) Non-chondritic HSE budget in Earth's upper mantle evidenced by abyssal peridotites from Gakkel ridge (Arctic Ocean). *Earth Planet. Sci. Lett.* **283**(1–4), 122–132.

Liu C. Z., Snow J. E., Hellebrand E., Brügmann G., Von Der Handt A., Büchl A. and Hofmann A. W. (2008) Ancient, highly heterogeneous mantle beneath Gakkel ridge. *Arctic Ocean. Nature* **452**(7185), 311–316.

Lorand J. P. and Luguet A. (2016) Chalcophile and siderophile elements in mantle rocks: Trace elements controlled by trace minerals. *Rev. Mineral. Geochem.* **81**(1), 441–488.

Luguet A. and Pearson G. (2019) Dating mantle peridotites using Re-Os isotopes: The complex message from whole rocks, base metal sulfides, and platinum group minerals. *Am. Mineralogist: J. Earth Planet. Mater.* **104**(2), 165–189.

Luguet A. and Reisberg L. (2016) Highly siderophile element and ^{187}Os signatures in non-cratonic basalt-hosted peridotite xenoliths: Unravelling the origin and evolution of the post-Archean lithospheric mantle. *Rev. Mineral. Geochem.* **81**(1), 305–367.

Luguet A., Lorand J. P. and Seyler M. (2003) Sulfide petrology and highly siderophile element geochemistry of abyssal peridotites: A coupled study of samples from the Kane Fracture Zone (45° W 23°20N, MARK area, Atlantic Ocean). *Geochim. Cosmochim. Acta* **67**(8), 1553–1570.

Luguet A., Alard O., Lorand J. P., Pearson N. J., Ryan C. and O'Reilly S. Y. (2001) Laser-ablation microprobe (LAM)-ICPMS unravels the highly siderophile element geochemistry of the oceanic mantle. *Earth Planet. Sci. Lett.* **189**(3–4), 285–294.

Maas C., Manske L., Wünnemann K. and Hansen U. (2021) On the fate of impact-delivered metal in a terrestrial magma ocean. *Earth Planet. Sci. Lett.* **554** 116680.

Maier W. D., Barnes S. J., Campbell I. H., Fiorentini M. L., Peltonen P., Barnes S. J. and Smithies R. H. (2009) Progressive mixing of meteoritic veneer into the early Earth's deep mantle. *Nature* **460**(7255), 620–623.

Malvoisin B. (2015) Mass transfer in the oceanic lithosphere: serpentinization is not isochemical. *Earth Planet. Sci. Lett.* **430**, 75–85.

Marchesi C., Dale C. W., Garrido C. J., Pearson D. G., Bosch D., Bodinier J. L., Gervilla F. and Hidas K. (2014) Fractionation of highly siderophile elements in refertilized mantle: Implications for the Os isotope composition of basalts. *Earth Planet. Sci. Lett.* **400**, 33–44.

Marchi S., Canup R. M. and Walker R. J. (2018) Heterogeneous delivery of silicate and metal to the Earth by large planetesimals. *Nat. Geosci.* **11**(1), 77–81.

Martin C. E. (1991) Osmium isotopic characteristics of mantle-derived rocks. *Geochim. Cosmochim. Acta* **55**, 1421–1434.

McDonough W. F. and Sun S. S. (1995) The composition of the Earth. *Chemical geology* **120**(3–4), 223–253.

Meisel T. and Horan M. F. (2016) Analytical methods for the highly siderophile elements. *Rev. Mineral. Geochem.* **81**(1), 89–106.

Meisel T., Walker R. J. and Morgan J. W. (1996) The osmium isotopic composition of the Earth's primitive upper mantle. *Nature* **383**(6600), 517–520.

Morgan J. W. (1986) Ultramafic xenoliths: clues to Earth's late accretionary history. *J. Geophys. Res. Solid Earth* **91**(B12), 12375–12387.

Morgan J. W., Walker R. J., Brandon A. D. and Horan M. F. (2001) Siderophile elements in Earth's upper mantle and lunar breccias: data synthesis suggests manifestations of the same late influx. *Meteorit. Planet. Sci.* **36**(9), 1257–1275.

Mundl-Petermeier A., Walker R. J., Fischer R. A., Lekic V., Jackson M. G. and Kurz M. D. (2020) Anomalous ^{182}W in high ^{3}He/^{4}He ocean island basalts: Fingerprints of Earth's core? *Geochim. Cosmochim. Acta* **271**, 194–211.

Mundl-Petermeier A., Walker R. J., Jackson M. G., Blichert-Toft J., Kurz M. D. and Halldórsson S. A. (2019) Temporal evolution of primordial tungsten-182 and ^{3}He/^{4}He signatures in the Iceland mantle plume. *Chem. Geol.* **525**, 245–259.

Mundl A., Touboul M., Jackson M. G., Day J. M. D., Kurz M. D., Lekic V., Helz R. T. and Walker R. J. (2017) Tungsten-182 heterogeneity in modern ocean island basalts. *Science* **356** (6333), 66–69.

Murthy V. R. (1991) Early differentiation of the Earth and the problem of mantle siderophile elements: a new approach. *Science* **253**(5017), 303–306.

Niu Y. (2004) Bulk-rock major and trace element compositions of abyssal peridotites: implications for mantle melting, melt extraction and post-melting processes beneath mid-ocean ridges. *J. Petrol.* **45**(12), 2423–2458.

O'Driscoll B., Walker R. J., Day J. M. D., Ash R. D. and Daly J. S. (2015) Generations of melt extraction, melt–rock interaction and high-temperature metasomatism preserved in peridotites of the ~497 Ma Leka Ophiolite Complex, Norway. *J. Petrology* **56**(9), 1797–1828.

O'Driscoll B., Day J. M. D., Walker R. J., Daly J. S., McDonough W. F. and Piccoli P. M. (2012) Chemical heterogeneity in the upper mantle recorded by peridotites and chromitites from the Shetland Ophiolite Complex, Scotland. *Earth Planet. Sci. Lett.* **333**, 226–237.

O'Neill H. S. C., Dingwell D. B., Borisov A., Spettel B. and Palme H. (1995) Experimental petrochemistry of some highly siderophile elements at high temperatures, and some implications for core formation and the mantle's early history. *Chem. Geol.* **120**(3–4), 255–273.

Paquet M., Cannat M., Brunelli D., Hamelin C. and Humler E. (2016) Effect of melt/mantle interactions on MORB chemistry at the easternmost Southwest Indian Ridge (61°–67°E). *Geochem. Geophys. Geosyst.* **17**(11), 4605–4640.

Parkinson I. J., Hawkesworth C. J. and Cohen A. S. (1998) Ancient mantle in a modern arc: Osmium isotopes in Izu-Bonin-Mariana forearc peridotites. *Science* **281**(5385), 2011–2013.

Paulick H., Bach W., Godard M., De Hoog J. C. M., Suhr G. and Harvey J. (2006) Geochemistry of abyssal peridotites (Mid-Atlantic Ridge, 15°20′N, ODP Leg 209): implications for fluid/rock interaction in slow spreading environments. *Chem. Geol.* **234**(3–4), 179–210.

Peters B.J., Mundl-Petermeier A., Carlson R.W., Walker R.J. and Day J.M.D., Combined Lithophile-Siderophile Isotopic Constraints on Hadean Processes Preserved in Ocean Island Basalt Sources, *Geochem., Geophys., Geosyst.*, **22** (3), 2021, e2020GC009479.

Peters B. J., Day J. M. D. and Taylor L. A. (2016) Early mantle heterogeneities in the Réunion hotspot source inferred from highly siderophile elements in cumulate xenoliths. *Earth Planet. Sci. Lett.* **448**, 150–160.

Rehkämper M., Halliday A. N., Fitton J. G., Lee D. C., Wieneke M. and Arndt N. T. (1999) Ir, Ru, Pt, and Pd in basalts and komatiites: new constraints for the geochemical behavior of the platinum-group elements in the mantle. *Geochim. Cosmochim. Acta* **63**(22), 3915–3934.

Reisberg L. (2021) Osmium isotope constraints on formation and refertilization of the non-cratonic continental mantle lithosphere. *Chem. Geol.* **574** 120245.

Reisberg L. and Lorand J. P. (1995) Longevity of sub-continental mantle lithosphere from osmium isotope systematics in orogenic peridotite massifs. *Nature* **376**(6536), 159–162.

Ringwood A. E. (1977) Composition of the core and implications for origin of the Earth. *Geochem. J.* **11**(3), 111–135.

Rizo H., Walker R. J., Carlson R. W., Horan M. F., Mukhopadhyay S., Manthos V. and Jackson M. G. (2016) Preservation of Earth-forming events in the tungsten isotopic composition of modern flood basalts. *Science* **352**(6287), 809–812.

Rouméjon S. (2014) Serpentinisation des péridotites exhumées aux dorsales lentes : approches microstructurale, minéralogique et géochimique. *Institut de Physique du Globe de Paris*.

Roy-Barman M. and Allègre C. J. (1994) $^{187}Os/^{186}Os$ ratios of mid-ocean ridge basalts and abyssal peridotites. *Geochim. Cosmochim. Acta* **58**(22), 5043–5054.

Sanfilippo A., Salters V., Tribuzio R. and Zanetti A. (2019) Role of ancient, ultra-depleted mantle in Mid-Ocean-Ridge magmatism. *Earth Planet. Sci. Lett.* **511**, 89–98.

Schulte R. F., Schilling M., Anma R., Farquhar J., Horan M. F., Komiya T., Farquhar J., Piccoli P. M., Pitcher L. and Walker R. J. (2009) Chemical and chronologic complexity in the convecting upper mantle: Evidence from the Taitao ophiolite, southern Chile. *Geochim. Cosmochim. Acta* **73**(19), 5793–5819.

Seyler M., Lorand J. P., Toplis M. J. and Godard G. (2004) Asthenospheric metasomatism beneath the mid-ocean ridge: Evidence from depleted abyssal peridotites. *Geology* **32**(4), 301–304.

Seyler M., Cannat M. and Mével C. (2003) Evidence for major-element heterogeneity in the mantle source of abyssal peridotites from the Southwest Indian Ridge (52° to 68°E). *Geochem. Geophys. Geosyst.* **4**(2).

Sichel S. E., Esperanca S., Motoki A., Maia M., Horan M. F., Szatmari P., da Costa Alves E. and Mello S. L. M. (2008) Geophysical and geochemical evidence for cold upper mantle beneath the equatorial Atlantic Ocean. *Rev. Bras. Geofis.* **26**, 69–86.

Snortum E. and Day J. M. D. (2020) Forearc origin for Coast Range Ophiolites inferred from osmium isotopes and highly siderophile elements. *Chem. Geol.* **550** 119723.

Snortum E., Day J. M. D. and Jackson M. G. (2019) Pacific lithosphere evolution inferred from Aitutaki mantle xenoliths. *J. Petrol.* **60**(9), 1753–1772.

Snow J. E. and Dick H. J. (1995) Pervasive magnesium loss by marine weathering of peridotite. *Geochim. Cosmochim. Acta* **59** (20), 4219–4236.

Snow J. E. and Reisberg L. (1995) Os isotopic systematics of the MORB mantle: results from altered abyssal peridotites. *Earth Planet. Sci. Lett.* **133**(3–4), 411–421.

Snow J. E. and Schmidt G. (1998) Constraints on Earth accretion deduced from noble metals in the oceanic mantle. *Nature* **391** (6663), 166–169.

Standish J. J., Hart S. R., Blusztajn J., Dick H. J. B. and Lee K. L. (2002) Abyssal peridotite osmium isotopic compositions from Cr-spinel. *Geochem. Geophys. Geosyst.* **3**.

Stracke A., Snow J. E., Hellebrand E., von der Handt A., Bourdon B., Birbaum K. and Günther D. (2011) Abyssal peridotite Hf isotopes identify extreme mantle depletion. *Earth Planet. Sci. Lett.* **308**(3–4), 359–368.

Suer T.-A., Siebert J., Remusat L., Day J. M. D., Borensztajn S., Doisineau B. and Fiquet G. (2021) Reconciling metal-silicate partitioning and late accretion in the Earth. *Nat. Commun.* **12**, 2193.

Turekian K. K. and Clark, Jr, S. P. (1969) Inhomogeneous accumulation of the Earth from the primitive solar nebula. *Earth Planet. Sci. Lett.* **6**(5), 346–348.

Van de Löcht J., Hoffmann J. E., Li C., Wang Z., Becker H., Rosing M. T. and Münker C. (2018) Earth's oldest mantle peridotites show entire record of late accretion. *Geology* **46**(3), 199–202.

Walker R. J., Carlson R. W., Shirey S. B. and Boyd F. R. (1989) Os, Sr, Nd, and Pb isotope systematics of southern African peridotite xenoliths: implications for the chemical evolution of subcontinental mantle. *Geochim. Cosmochim. Acta* **53**(7), 1583–1595.

Wänke H. (1981) Constitution of terrestrial planets. *Philos. Trans. Royal Soc. London. Ser. A, Math. Phys. Sci.* **303**(1477), 287–302.

Warren J. M. (2016) Global variations in abyssal peridotite compositions. *Lithos* **248**, 193–219.

Warren J. M., Shimizu N., Sakaguchi C., Dick H. J. B. and Nakamura E. (2009) An assessment of upper mantle heterogeneity based on abyssal peridotite isotopic compositions. *J. Geophys. Res. Solid Earth* **114**(B12).

Waterton P., Mungall J. and Pearson D. G. (2021) The komatiite-mantle platinum-group element paradox. *Geochim. Cosmochim. Acta*.

Willbold M., Elliott T. and Moorbath S. (2011) The tungsten isotopic composition of the Earth's mantle before the terminal bombardment. *Nature* **477**(7363), 195–198.

Zhang C., Liu C. Z., Ji W. B., Liu T. and Wu F. Y. (2020) Heterogeneous sub-ridge mantle of the Neo-Tethys: Constraints from Re-Os isotope and HSE compositions of the Xigaze ophiolites. *Lithos* **105819**.

Associate editor: Andreas Stracke